Stochastic linearization of turbulent dynamics of dispersive waves in equilibrium and non-equilibrium state

2016 New J. Phys. 18 083028

(http://iopscience.iop.org/1367-2630/18/8/083028)

New Journal of Physics
The open access journal at the forefront of physics

Deutsche Physikalische Gesellschaft DPG
IOP Institute of Physics

Published in partnership with: Deutsche Physikalische Gesellschaft and the Institute of Physics

OPEN ACCESS

RECEIVED
8 March 2016

REVISED
22 July 2016

ACCEPTED FOR PUBLICATION
25 July 2016

PUBLISHED
8 August 2016

PAPER

Stochastic linearization of turbulent dynamics of dispersive waves in equilibrium and non-equilibrium state

Shixiao W Jiang[1], **Haihao Lu**[1], **Douglas Zhou**[1,4] **and David Cai**[1,2,3,4]

[1] School of Mathematical Sciences, MOE-LSC, and Institute of Natural Sciences, Shanghai Jiao Tong University, Shanghai 200240, People's Republic of China
[2] Courant Institute of Mathematical Sciences and Center for Neural Science, New York University, New York, NY 10012, USA
[3] NYUAD Institute, New York University Abu Dhabi, PO Box 129188, Abu Dhabi, United Arab Emirates
[4] Authors to whom any correspondence should be addressed.

E-mail: zdz@sjtu.edu.cn **and** cai@cims.nyu.edu

Keywords: effective linear stochastic structure, β-Fermi–Pasta–Ulam chain, nonequilibrium steady state, long-wavelength renormalized waves

Abstract

Characterizing dispersive wave turbulence in the long time dynamics is central to understanding of many natural phenomena, e.g., in atmosphere ocean dynamics, nonlinear optics, and plasma physics. Using the β-Fermi–Pasta–Ulam nonlinear system as a prototypical example, we show that in thermal equilibrium and non-equilibrium steady state the turbulent state even in the strongly nonlinear regime possesses an effective linear stochastic structure in renormalized normal variables. In this framework, we can well characterize the spatiotemporal dynamics, which are dominated by long-wavelength renormalized waves. We further demonstrate that the energy flux is nearly saturated by the long-wavelength renormalized waves in non-equilibrium steady state. The scenario of such effective linear stochastic dynamics can be extended to study turbulent states in other nonlinear wave systems.

1. Introduction

Dispersion relations play a controlling role in characterizing turbulence of weakly nonlinear dispersive waves [1]. For strongly nonlinear waves in thermal equilibrium and non-equilibrium, is there a similar relation that can capture important dynamic features of the turbulence? It has been found that such relations, referred to as renormalized dispersion relations, often arise from wave–wave interactions, and they can deviate substantially from the bare linear dispersion relation [2–6]. The pioneering Fermi–Pasta–Ulam (FPU) lattice is an example exhibiting such phenomenon even in strongly nonlinear regimes [2, 3, 6–9]. The FPU lattice problem has spurred a great number of important developments in physics and mathematics [10, 11]. There have been many theoretical and numerical efforts in understanding its anomalous heat conduction, i.e., the divergence of the thermal conductivity and the failure of Fourier's law [12–15] as the problem of energy transport in one dimensional systems has attracted great interests in recent decades [12, 16]. Here, one has to address important questions of what are the carriers that transport energy in turbulent states and what are their spatiotemporal characteristics in both thermal equilibrium and nonequilibrium steady state. In this work, we will address these issues through characterizing spatiotemporal features of these carriers using the renormalized dispersion relation and show that energy transport in the turbulent state is controlled by the renormalized waves. Resolution of these issues can provide deep insights into effective descriptions of turbulent states in general nonlinear dispersive waves in thermal equilibrium and nonequilibrium steady state.

We will show below that there is a linear stochastic dynamic structure embedded in the β-FPU turbulent states in thermal equilibrium even in strongly nonlinear regimes. This linear structure is intimately related to the renormalized dispersion relation. By examining the spatiotemporal characteristics and dynamical behaviors of renormalized waves, we demonstrate that the long time behavior of the momentum correlation functions is dominated by the long-wavelength renormalized waves and the linear stochastic structure results in a power-law

decay of the amplitude of momentum correlation functions [17–20]. We further show that these dynamical features of renormalized waves persist in nonequilibrium steady state turbulence. We demonstrate that the energy carriers in nonequilibrium steady state are long-wavelength renormalized waves in the linear stochastic dynamic structure, which nearly saturates the total energy flux in the turbulence. This scenario of linear stochastic dynamic structure characterized by the renormalized dispersion relation can be extended to the turbulence descriptions of many general nonlinear wave systems in both thermal equilibrium and nonequilibrium steady state.

2. The FPU model

The dimensionless Hamiltonian of the β-FPU chain is

$$H = \sum_{n=-N/2+1}^{N/2} \frac{1}{2}p_n^2 + \frac{1}{2}(q_{n+1} - q_n)^2 + \frac{\beta}{4}(q_{n+1} - q_n)^4, \tag{1}$$

where p_n and q_n are the momentum and the displacement of the nth particle, respectively, and β parameterizes the strength of nonlinearity. In the Fourier space, the Hamiltonian can be written as

$$H = \sum_{k=0}^{N-1} \frac{1}{2}\ |P_k|^2 + \frac{1}{2}\omega_k^2\ |Q_k|^2 + V(Q),$$

where

$$\omega_k = 2\sin\left(\frac{k\pi}{N}\right) \tag{2}$$

is the linear dispersion relation, P_k, Q_k and $V(Q)$ are the Fourier transforms of p_n, q_n and the quartic term, respectively. To investigate the β-FPU system in equilibrium, we apply the periodic boundary conditions. For nonequilibrium steady state, we apply fixed boundary conditions $q_{-N/2} = q_{N/2+1} = 0$. The particles of $n = -N/2 + 1$ and $n = N/2$ at two ends are connected to Langevin heat reservoirs; i.e., with the governing equations $\ddot{q}_n = -\partial H/\partial q_n - \lambda\dot{q}_n + \sigma_n\xi_n(t)$, where $\xi_n(t)$ is Guassian white noise with $\langle\xi_n(t)\rangle = 0$, $\langle\xi_n(t)\xi_n(t')\rangle = \delta(t - t')$. The driving coefficients σ_n and the dissipation coefficient λ satisfy the Einstein relation $\sigma_n^2 = 2\lambda T_n$, where T_n are the temperatures of the two heat reservoirs.

2.1. Renormalized dispersion relation

In thermal equilibrium, the renormalized dispersion relation has been obtained from an exact linear Langevin equation (LLE) in the Zwanzig–Mori projection framework [21, 22]:

$$(\omega_k^Z)^2 = \frac{\left\langle \dfrac{\partial H}{\partial Q_k^*} Q_k^* \right\rangle}{\langle |Q_k|^2 \rangle}, \tag{3}$$

where $\langle\cdot\rangle$ denotes thermal average, and is interpreted as a long time average in numerical computation. By employing the energy equipartition theorem in the renormalized dispersion relation (3), ω_k^Z can be written as

$$\omega_k^L = \sqrt{\frac{\langle K\rangle}{\langle U\rangle}}\,\omega_k \equiv \eta_L\omega_k, \tag{4}$$

where $K = \sum_{n=-N/2+1}^{N/2} p_n^2/2$ and $U = \sum_{n=-N/2+1}^{N/2}(q_{n+1} - q_n)^2/2$ are the kinetic and quadratic potential energy, respectively, and η_L is a renormalization factor of the dispersion relation. Based on the equality $\langle K\rangle = \langle U\rangle + 2\langle V(Q)\rangle$ obtained from the equipartition theorem for the β-FPU chain, equation (4) can be written in the form of $\omega_k^L = \sqrt{1 + 2\langle V\rangle/\langle U\rangle}\,\omega_k$, which has the same form as proposed in [7, 8]. In figure 1, we display the measured dispersion relation $\Omega_k^{\rm meas}$. For a fixed mode k, the measured $\Omega_k^{\rm meas}$ corresponds to the value of ω on the $\omega - k$ plane where the spatiotemporal spectrum $|\widehat{Q}_k(\omega)|^2$ reaches its maximum value. Here, $\widehat{Q}_k(\omega)$ is the temporal Fourier transform of $Q_k(t)$. It is important to note that for both thermal equilibrium and nonequilibrium steady state, the theoretical prediction (4) agrees very well with $\Omega_k^{\rm meas}$ and these renormalized dispersion relations are induced by wave–wave resonances, instead of inherited from their linear dispersive dynamics [6, 9]. More specifically, the contribution of the trivial and nontrivial resonances is significant to the renormalization of the dispersion relation [9].

2.2. Spatiotemporal characteristics

We now turn to the question of how these renormalized dispersive waves manifest themselves spatially and temporally in the turbulent state of thermal equilibrium and nonequilibrium steady state. The columns of

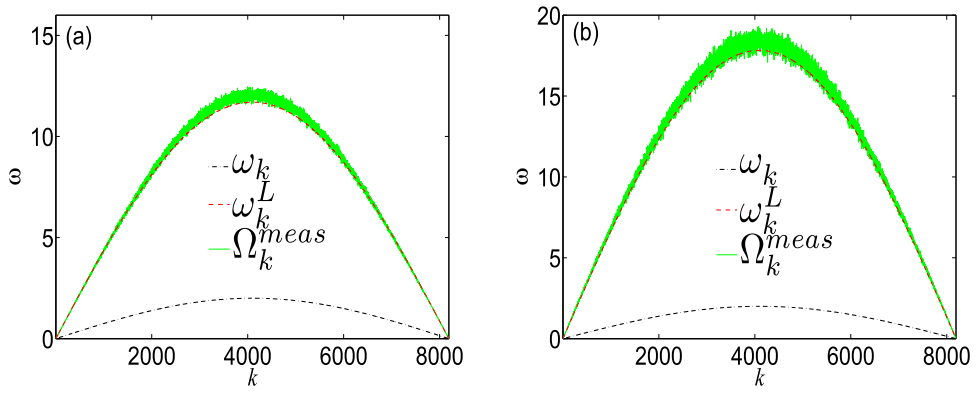

Figure 1. Comparison of dispersion relations ω_k^L, Ω_k^{meas}, and ω_k for the β-FPU chain with $N = 8192$ in (a) thermal equilibrium and (b) nonequilibrium steady state. The dashed–dotted black line corresponds to ω_k, the dashed red line corresponds to ω_k^L, and the solid green line corresponds to Ω_k^{meas}. In thermal equilibrium, the parameters are $\beta = 100$ and $H/N = 3.9$. In the nonequilibrium steady state, the parameters are $\beta = 100$, $\lambda = 1$, $\sigma_{-N/2+1} = 1$, and $\sigma_{N/2} = 10$.

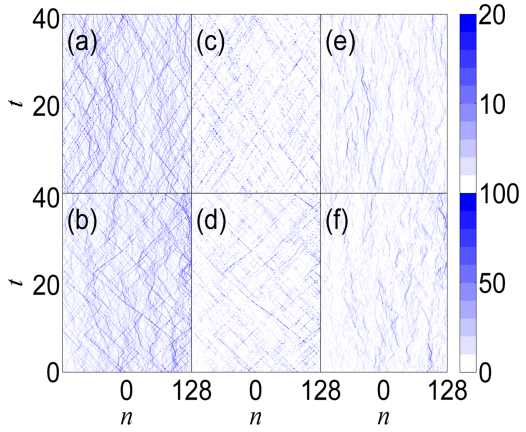

Figure 2. Spatiotemporal evolution of kinetic energy density for the β-FPU chains with $N = 256$ in thermal equilibrium (upper panel) and in nonequilibrium steady state (lower panel). The left (a) (b), middle (c) (d), and right (e) (f) columns correspond to $p_n^2/2$, $(p_n^{lk})^2/2$, and $(p_n^{hk})^2/2$, respectively (see text). The parameters $\beta, H/N, \lambda, \sigma_{-N/2+1}$, and $\sigma_{N/2}$ are the same as those in figure 1.

figure 2 display the kinetic energy density evolution $p_n^2/2$, $(p_n^{lk})^2/2$, and $(p_n^{hk})^2/2$, respectively, where the low k momentum $p_n^{lk} = \frac{1}{\sqrt{N}}\sum_{k\in K_L} P_k \exp(-\mathrm{i}2\pi kn/N)$ with $K_L = [0,\ N/4] \cup [3N/4,\ N-1]$ and the high k momentum $p_n^{hk} = \frac{1}{\sqrt{N}}\sum_{k\in K_H} P_k \exp(-\mathrm{i}2\pi kn/N)$ with $K_H = [N/4+1,\ 3N/4-1]$. In figures 2(a) and (b), two types of localized objects (dark stripes) that carry sufficiently large amount of kinetic energy can be clearly observed. For the ballistically traveling localized objects (nearly straight crosshatch stripes in figures 2(a) and (b)), it can be numerically examined that they move approximately at the speed of the renormalization factor η_L. Furthermore, the spatial structure of these objects resembles that of low k kinetic energy $(p_n^{lk})^2/2$ (figures 2(c) and (d)). These traveling localized objects are wave packets of low k renormalized dispersive waves. The other type of localized objects (meandering stripes in figures 2(a) and (b)) execute nearly random walks in space. They show similar behaviors as high k kinetic energy $(p_n^{hk})^2/2$ (figures 2(e) and (f)). Their temporal frequencies are near the high frequency edge of the renormalized dispersion band [2, 3]. These localized objects are wave packets of high k renormalized waves and have been identified as discrete breathers (DBs) because their spatial structure strongly resembles the idealized DBs in the β-FPU system [2, 3]. A numerical study analogous to figure 2(a) can be found in [23]. However, we emphasize here that there is a rather different spatiotemporal manifestation between long-wavelength and short-wavelength renormalized waves as can be seen from figure 2. Moreover, we demonstrate that the traveling localized objects in figures 2(c) and (d) correspond to wave packets of low k renormalized waves. As will be shown below, these objects dominate the long time behavior of the momentum correlation function and they are responsible for transporting energy in nonequilibrium steady state in the β-FPU system.

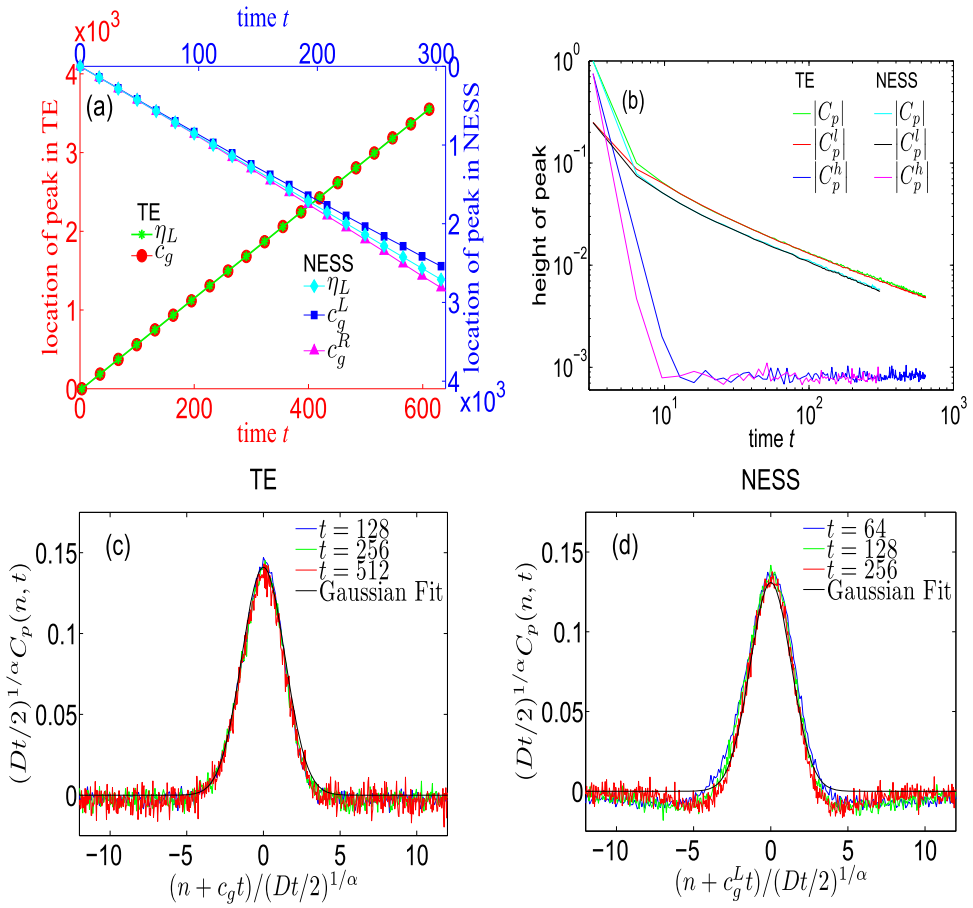

Figure 3. (a) Peak locations of $C_p(n,\ t)$ versus time t for the β-FPU chain in thermal equilibrium (TE) (red axis): theoretical predictions η_L (green stars) and numerical measurements of the left moving mode c_g (red circles). Also plotted are peak locations of $C_p(n,\ t)$ versus time t in nonequilibrium steady state (NESS) (blue axis): theoretical predictions η_L (cyan diamonds), numerical measurements of the left moving mode c_g^L (blue squares) and the right moving mode c_g^R (magenta triangles). (b) Decay of the amplitude of correlation functions in time: $C_p(n,\ t)$ (green), $C_{p^l}(n,\ t)$ (red), and $C_{p^h}(n,\ t)$ (blue) for the β -FPU chain in thermal equilibrium. In nonequilibrium steady state, their colors are cyan, black, and magenta, respectively. (c) and (d) scaling of the spatial profile of $C_p(n,\ t)$: scaled plots of the left moving mode $C_p(n,\ t)$ at different times in thermal equilibrium and nonequilibrium steady state, respectively. For comparison, also plotted are the corresponding Guassian fits. The fitting parameter D is 2.6 in thermal equilibrium and 2.0 in nonequilibrium steady state. The particle number is $N = 8192$. The parameters $\beta, H/N, \lambda, \sigma_{-N/2+1}$, and $\sigma_{N/2}$ are the same as those in figure 1.

2.3. Dynamical behaviors of the momentum correlation

To further characterize the dynamical behaviors of these renormalized dispersive waves, we invoke the momentum correlation function [17]

$$C_p(n,\ t) = \frac{\langle p_n(t) p_0(0)\rangle}{\langle p_0(0) p_0(0)\rangle}, \tag{5}$$

which describes the spatiotemporal evolution of momentum fluctuations. For the turbulent state in both thermal equilibrium and nonequilibrium steady state, we can numerically show that $C_p(n,\ t)$ possesses the following properties: (i) the peak location of $C_p(n,\ t)$ can be well described by $\eta_L t$, i.e., moving at the group velocity, c_g, of renormalized waves (as shown in figure 3(a)), where the group velocity is determined by the renormalized waves $c_g = \partial\omega_k^L/\partial(2\pi k/N)|_{k\to 0} = \eta_L$. (ii) There is a power-law decay of the amplitude of $C_p(n,\ t)$ as shown in figure 3(b). For comparison, figure 3(b) also displays the amplitude of $C_{p^l}(n,\ t)$ and $C_{p^h}(n,\ t)$, where $C_{p^l}(n,\ t)$ and $C_{p^h}(n,\ t)$ are correlation functions of p_n^{lk} and p_n^{hk}, respectively. It can be seen that for sufficiently large time, $|C_p^l|$ decays at the same rate as $|C_p|$ whereas $|C_p^h|$ decays much rapidly. This demonstrates that the dynamical behaviors of the ballistically traveling wave packets are indeed controlled by the low k renormalized waves. (iii) $C_p(n,\ t)$ possesses a Gaussian profile in space as shown in figure 3(c).

3. Effective linear stochastic structure

Next, we discuss that there is an effective linear dynamics underlying properties (i)–(iii) in the β-FPU turbulent states. We first discuss the equilibrium dynamics. Applying the Zwanzig–Mori formalism [21, 22], one can rewrite the nonlinear β-FPU dynamics in equilibrium to obtain an exact LLE [6, 13, 14]. Under the Markovian approximation [13, 14], the LLE can reduce to an effective linear dynamics of the renormalized waves with the renormalized dispersion relation ω_k^L:

$$\begin{aligned} \dot{Q}_k(t) &= P_k(t), \\ \dot{P}_k(t) &= -(\omega_k^L)^2 Q_k(t) - \gamma_k P_k(t) + R_k(t), \end{aligned} \tag{6}$$

where $R_k(t)$ is a white noise with $\langle R_k(t)\rangle = 0$, $\langle R_k(t)R_k^*(t')\rangle = 2\gamma_k T\delta(t-t')$ with T the temperature. The linear dynamics (6) gives rise to the momentum spectrum,

$$S_{P_k}(\omega) \equiv \langle |P_k(\omega)|^2\rangle = \frac{2\omega^2\gamma_k T}{((\omega_k^L)^2 - \omega^2)^2 + \gamma_k^2\omega^2}.$$

In the limit of $N \to \infty$, the corresponding correlation function $C_p(n, t)$ becomes

$$\begin{aligned} C_p(n,t) = &\frac{1}{2\pi}\int_0^\pi e^{-\frac{\gamma_k}{2}t}\left[\cos\phi^+ - \frac{\gamma_k}{2\widetilde{\omega}_k^L}\sin\phi^+\right]dk \\ &+ \frac{1}{2\pi}\int_0^\pi e^{-\frac{\gamma_k}{2}t}\left[\cos\phi^- - \frac{\gamma_k}{2\widetilde{\omega}_k^L}\sin\phi^-\right]dk, \end{aligned} \tag{7}$$

where $\phi^+ = \widetilde{\omega}_k^L t + kn$, $\phi^- = \widetilde{\omega}_k^L t - kn$, and $\widetilde{\omega}_k^L = \sqrt{(\omega_k^L)^2 - \gamma_k^2/4}$. The first integral and the second integral in equation (7) arise from the left moving and right moving renormalized waves, respectively. Next, we assume a scaling relation for the relaxation rate, $\gamma_k \sim Dk^\alpha$ in the limit of small wavenumbers. From our numerical examination, the relaxation rate γ_k can be directly computed from the decay rate of $\langle P_k(t)P_k^*(0)\rangle$ for low k's and then the value of α can be numerically extracted from such γ_k as 1.9 ± 0.1. There have been many studies about the value of the scaling exponent α [15, 18, 19, 24–28]. The value $\alpha = 2$, which is consistent with our simulation, is theoretically predicted by the mode-coupling theory [19, 28]. Under this scaling assumption, we obtain that for large t the integral (7) is asymptotically dominated by the contribution from $k \to 0$. In the moving frame $r = n \pm \eta_L t$ at large time, the asymptotic behavior of the left moving and right moving components of $C_p(n, t)$ is

$$C_p^{\mp}(n,t) \sim \frac{1}{2\pi\alpha}\frac{\Gamma\left(\frac{1}{\alpha}\right)}{\left(\frac{Dt}{2}\right)^{1/\alpha}}\exp\left(-\frac{1}{2}\frac{\Gamma\left(\frac{3}{\alpha}\right)}{\Gamma\left(\frac{1}{\alpha}\right)}\left[\frac{n \pm \eta_L t}{\left(\frac{Dt}{2}\right)^{1/\alpha}}\right]^2\right). \tag{8}$$

From equation (8), the peak locations are centered at site $n = \mp\eta_L t$ for left moving and right moving renormalized waves, respectively. Therefore, the group velocity c_g is indeed equal to the renormalization factor η_L, as consistent with what is observed in numerical experiment (figure 3(a)). Note that for our nonlinear waves the values of the renormalization factor η_L (figure 1(a)), the group velocity of low k renormalized waves (figure 2(c)) and the speed of the peak location of the correlation function $C_p(n, t)$ (figure 3(a)) are identical within numerical accuracy. Traditionally, one deals with the dispersion relation and the group velocity only for linear components of dispersive waves. For nonlinear waves, it is theoretically interesting to quantify their dispersion relation and group velocity and further understand the reason underlying above identities. We emphasize that the framework of the effective linear stochastic structure for nonlinear β-FPU systems provides a natural underpinning of the renormalization for the effective dispersion relation and its connection to the group velocity and the speed of the peak location of $C_p(n, t)$ in the nonlinear waves. The formula (8) displays a power-law decay in the amplitude, $|C_p| \sim t^{-1/\alpha}$. The value of α obtained from fitting of $|C_p| \sim t^{-1/\alpha}$ is 2.0 ± 0.1 in thermal equilibrium. These numerical results show that there is a self-consistency in our description of the effective linear dynamics. As the dominant contribution to the integral (7) comes from the neighborhood of $k = 0$ in the long time limit, only the low k modes contribute to the long time behaviors of $C_p(n, t)$ whereas the high k modes have a much shorter correlation time as shown in figure 3(b). Finally, our asymptotic analysis predicts a Gaussian profile for the scaled $C_p(n, t)$. Here, the scaled $C_p(n, t)$ is $(Dt/2)^{1/\alpha}C_p((n + c_g t)/(Dt/2)^{1/\alpha}, t)$, i.e., space is shifted by a distance $c_g t$, then scaled by $1/(Dt/2)^{1/\alpha}$, with amplitude scaled by $(Dt/2)^{1/\alpha}$. This Gaussian profile is confirmed in our numerical experiment, as shown in figure 3(c).

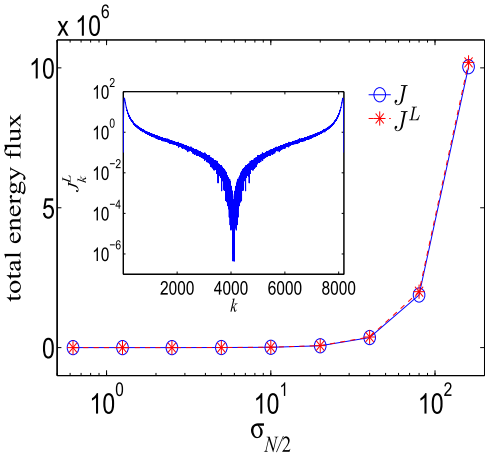

Figure 4. The energy flux as a function of the driving coefficient $\sigma_{N/2}$. Blue circles and red stars correspond to the energy flux J and the renormalized energy flux J^L, respectively. (Inset) The energy flux J_k^L versus wavenumber k. The particle number is $N = 8192$. The parameters β, λ, and $\sigma_{-N/2+1}$ are the same as those in figure 1.

4. Nonequilibrium steady state turbulence

Our numerical results of the turbulent states in nonequilibrium steady state with thermal reservoirs at the two ends are displayed in figures 2 and 3. Importantly, from these results, it can be clearly concluded that the above behaviors of renormalized dispersive waves persist and the prediction (8) is still valid (we note that the fitted value for α is 1.9 ± 0.1 in nonequilibrium steady state). Our previous work [9] has numerically confirmed that the theoretical renormalized dispersion relations are valid for a wide range of temperature gradients in nonequilibrium steady states. Therefore, the description of the effective linear dynamics (6) can be generalized to the nonequilibrium steady state turbulence for the β-FPU system. This effective description can be further corroborated by the following analysis of the energy flux. For a harmonic chain, the total energy flux J can be expressed in the Fourier space as $J = \mathrm{Im}\sum_{k=-N/2+1}^{N/2} J_k$, where $J_k = \langle \nu_k \omega_k Q_k P_k^* \rangle$ and $\nu_k = \cos(k\pi/N)$ is the group velocity. For the β-FPU turbulent state, we can show that the energy flux can be well approximated by $J^L = \mathrm{Im}\sum_{k=-N/2+1}^{N/2} J_k^L$, where J_k^L is obtained by assuming the linear wave system having the renormalized dispersion relation ω_k^L, i.e.,

$$J_k^L = \langle \nu_k^L \omega_k^L Q_k P_k^* \rangle, \tag{9}$$

with the corresponding renormalized $\nu_k^L = \eta_L \cos(k\pi/N)$. As can be seen from figure 4, for a wide range of driving strength $\sigma_{N/2}$, which is related to the temperature difference at the two ends, the total energy flux J^L of the linear system with the renormalized dispersion relation is in excellent agreement with the total energy flux of the original nonlinear dynamics $J = \sum_{n=-N/2+1}^{N/2} j_n$, where $j_n = \langle p_n[(q_{n+1} - q_n) + \beta(q_{n+1} - q_n)^3] \rangle$. Furthermore, we find that almost all contribution to the flux J^L comes from the low k modes (as seen in the inset of figure 4). The agreement between the renormalized flux J^L and J demonstrates that the renormalized waves in turbulence behave like nearly noninteracting linear waves in transporting energy and the energy carriers are wave packets of low k renormalized waves. Note that a decomposition of the flux into modal components can be naturally carried out for harmonic chains [14, 29]. However, our decomposition (9) is different from the decomposition $J_k = \langle \nu_k \omega_k Q_k P_k^* \rangle$ in early works [14] in the following sense. For nonlinear waves in anharmonic chains such as β-FPU chains, how to achieve a modal decomposition for flux is, in general, difficult. Here, because of the effective linear stochastic structure in nonlinear β-FPU chains, the flux can be well characterized by the decomposition (9) through renormalized components. As shown by the analysis of the contribution to the flux from each mode component J_k^L, we emphasize that low k renormalized waves are responsible for transporting energy in nonequilibrium steady state. From the above discussion, we can conclude that the ballistic traveling wave packets manifested in the turbulence are long-wavelength renormalized waves, characterized by a power-law correlation, traveling at the group velocity determined by the renormalized dispersion relation, and transporting energy in turbulence in nonequilibrium steady state as well.

5. Conclusion and discussion

We have examined the validity of effective linear stochastic dynamics in the strongly nonlinear regime of the β-FPU turbulence in both thermal equilibrium and nonequilibrium steady state. Using the effective linear

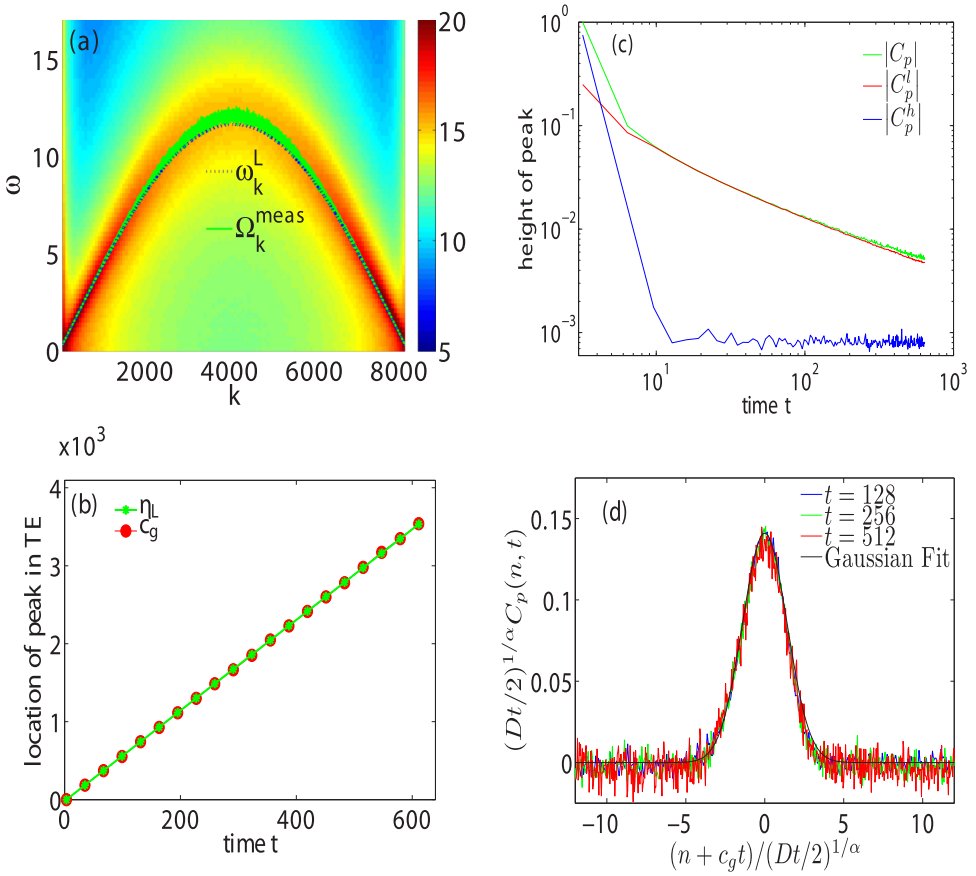

Figure 5. (a) Comparison of dispersion relations ω_k^L (dotted blue line) and $\Omega_k^{\rm meas}$ (solid green line) for the purely quartic chain with $N = 8192$ in thermal equilibrium. Plotted is the logarithmic modulus $\ln|\widehat{Q}_k(\omega)|^2$ with its magnitude color coded. The parameters are $\beta = 100$ and $H/N = 3.9$. (b) Peak locations of $C_p(n,\ t)$ versus time t. (c) Decay of the amplitude of correlation functions in time. (d) Scaling of the spatial profile of $C_p(n,\ t)$. The fitting parameter α is 2.0 and D is 2.6.

structure, we have well captured the long time behaviors of $C_p(n,\ t)$, including the group velocity and power-law decay of the amplitude. We have also demonstrated that the long time behavior of $C_p(n,\ t)$ is dominated by the long-wavelength renormalized waves. In addition, we have shown that the total energy flux is nearly saturated by long-wavelength renormalized waves, which constitute the energy carriers in the system. In the following, we further demonstrate that this scenario of linear stochastic dynamics can be generalized to other nonlinear wave systems. We first consider a purely quartic chain with the Hamiltonian $H = \sum_{n=-N/2+1}^{N/2} \frac{1}{2}p_n^2 + \frac{\beta}{4}(q_{n+1} - q_n)^4$. We emphasize that the linear dispersion relation is absent in this dynamics. However, the renormalized dispersion relation can be induced by the nonlinear wave interactions in thermal equilibrium (figure 5(a)). As shown in figure 5, the dynamical behaviors of renormalized dispersive waves in the turbulent state are the same as those in the β-FPU chain. In this turbulent state, the group velocity is also derived from the renormalized dispersion relation $\omega_k^L = 2\eta_L \sin(k\pi/N)$ with $\eta_L = \sqrt{\langle K\rangle/\langle U\rangle}$ (figure 5(b)) and there is a power-law decay of the correlation amplitude (figure 5(c)). It can be seen from figures 5(c) and (d) that the long time behavior of $C_p(n,\ t)$ is dominated by the long-wavelength renormalized waves as well. Therefore, the turbulence of the (dispersionless) purely quartic chain can be well captured by the effective linear stochastic structure with an induced renormalized dispersion relation ω_k^L. In contrast to many other one-dimensional momentum-conserving systems, the coupled rotator model exhibits a normal heat conduction [30, 31]. The coupled rotator model is described by the Hamiltonian $H = \sum_{n=-N/2+1}^{N/2} \frac{1}{2}p_n^2 + [1 - \cos(q_{n+1} - q_n)]$. In both the low and high energy limits, this dynamical system becomes integrable [14]. We here focus on the validity of the effective linear stochastic structure in its strongly chaotic, turbulent regime. It can be observed from figure 6(a) that both the measured dispersion relation $\Omega_k^{\rm meas}$ and the theoretical prediction $\omega_k^Z = \sqrt{\langle Q_k^* \partial H/\partial Q_k^*\rangle/\langle|Q_k|^2\rangle}$ vanish in the turbulent state (we note that there is a vestigial spectral band at the bare linear dispersion relation as can be observed faintly in figure 6(a). However, the spectral power at the renormalized dispersion relation $\omega_k^Z = 0$ is seven orders of magnitude higher than that at the bare linear dispersion band. Here, as usual, the bare linear dispersion relation can be obtained from the quadratic approximation of the Hamiltonian when $q_{n+1} - q_n$ is small). Because of the vanishing renormalized

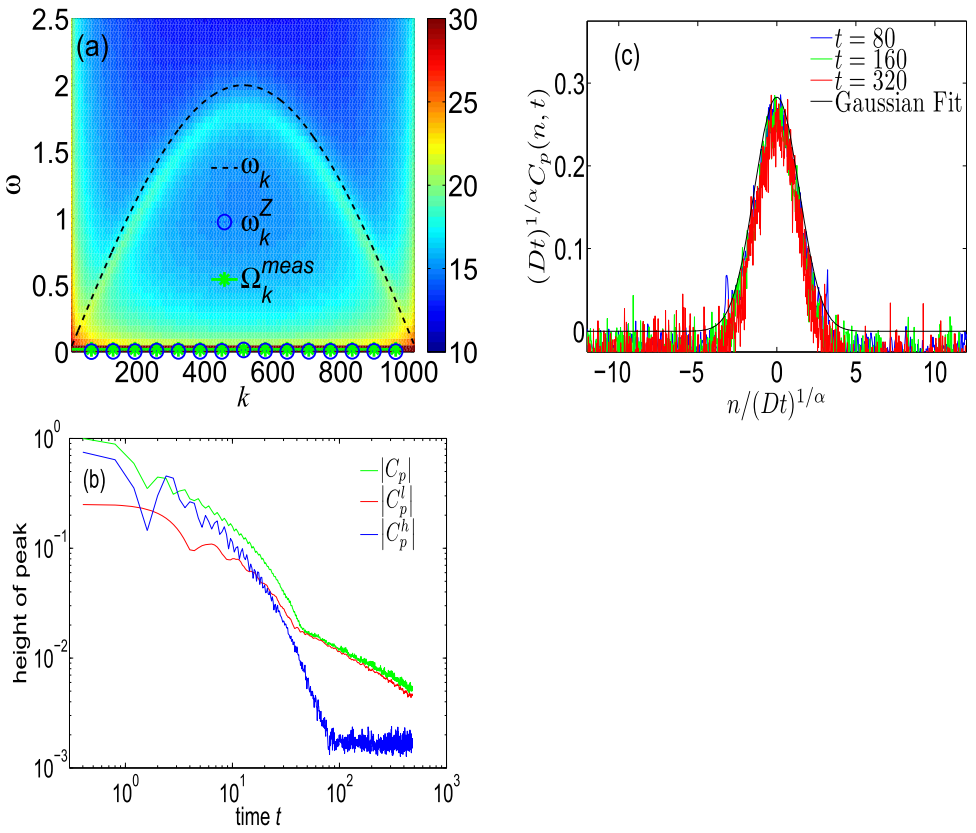

Figure 6. (a) Comparison of dispersion relations ω_k^Z (blue circles), $\Omega_k^{\rm meas}$ (green stars), and ω_k (dashed line) for the coupled rotator model with $N = 1024$ in thermal equilibrium. Plotted is the logarithmic modulus $\ln |\widehat{Q}_k(\omega)|^2$ with its magnitude color coded. The energy density is $H/N = 0.5$. (b) Decay of the amplitude of correlation functions in time. (c) Scaling of the spatial profile of $C_p(n,\, t)$. The fitting parameter α is 2.0 and D is 5.6.

dispersion relation, $\omega_k^Z = 0$, the linear stochastic structure gives rise to the asymptotic behavior of $C_p(n,\, t)$

$$C_p(n,\, t) \sim \frac{1}{\pi\alpha}\frac{\Gamma\left(\frac{1}{\alpha}\right)}{(Dt)^{1/\alpha}} \exp\left(-\frac{1}{2}\frac{\Gamma\left(\frac{3}{\alpha}\right)}{\Gamma\left(\frac{1}{\alpha}\right)}\left[\frac{n}{(Dt)^{1/\alpha}}\right]^2\right) \tag{10}$$

if the relaxation rate in the limit of small wavenumbers is assumed to be $\gamma_k \sim Dk^\alpha$. The long time behavior of $C_p(n,\, t)$ is again dominated by the long waves (figure 6(b)). Moreover, the form (10) with the parameter $\alpha = 2.0$ in $C_p(n,\, t)$ (figure 6(c)) signifies the diffusion of the momentum within the turbulence as confirmed in figure 6(c). Therefore, the turbulent states in all the above wave dynamics even without dispersion, regardless the conservation of momentum, can be successfully captured by the effective linear stochastic dynamics.

In addition to symmetric potentials as above, we further consider an asymmetric potential, i.e., the $\alpha\beta$-FPU chain with the Hamiltonian $H = \sum_{n=-N/2+1}^{N/2} \frac{1}{2}p_n^2 + \frac{1}{2}(q_{n+1} - q_n)^2 + \frac{\alpha'}{3}(q_{n+1} - q_n)^3 + \frac{\beta}{4}(q_{n+1} - q_n)^4$. If $\alpha' \neq 0$, the pressure typically is nonzero in the chain. The Boltzmann factor in this case is given by $\exp(-[V(x) + Px]/T)$, where T is the temperature, $x = q_{n+1} - q_n$, $V(x)$ is the potential of the chain, and P is the pressure [19]. In the NPT ensemble, the pressure $P = -\langle V'(x)\rangle_{P,T}$ can be viewed as an average force on a specific particle x. From the Boltzmann factor, we can see that the equilibrium position of x is not located at zero, but at x_0 with x_0 satisfying $V'(x_0) = -P$. If there is a unique solution of x_0, then in the low temperature regime the effective potential $V^{\rm eff}$ of renormalized waves is provided by $V^{\rm eff} = V(x) + Px = V(x_0) + V''(x_0)(x - x_0)^2/2 + V'''(x_0)(x - x_0)^3/3 + \beta(x - x_0)^4/4$ and the renormalization factor η_L is

$$\eta_L = \sqrt{\frac{\langle K\rangle}{\langle \widetilde{U}\rangle}} \text{ with } \widetilde{U} = \frac{1}{2}\sum_{n=-N/2+1}^{N/2}(q_{n+1} - q_n - x_0)^2, \tag{11}$$

where x_0 satisfies the equation $V'(x_0) = \langle V'(q_{n+1} - q_n)\rangle_{P,T}$. From figure 7(a), we can clearly see that the theoretical prediction is in excellent agreement with the measured dispersion relation. There is a power-law decay of the correlation amplitude (figure 7(c)). The fitting parameter $\alpha = 1.6$ so that the decay rate of correlation amplitude is 0.62 which is close to the result 2/3 predicted in [18–20]. The long time behavior of $C_p(n,\, t)$ is again dominated by the long-wavelength renormalized waves (figures 7(c) and (d)). Note that the

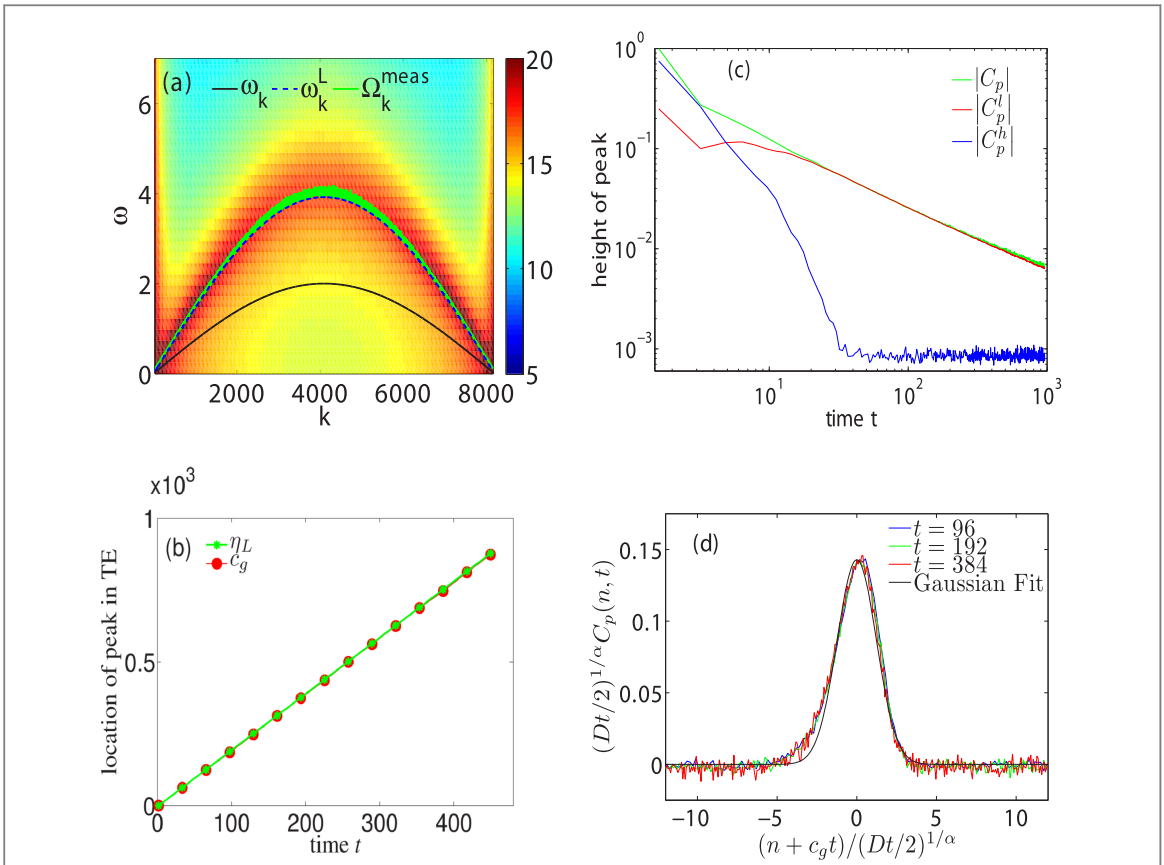

Figure 7. (a) Comparison of dispersion relations ω_k^L (dashed blue line), Ω_k^{meas} (solid green line), and ω_k (solid black line) for the $\alpha\beta$-FPU chain with $N = 8192$ in thermal equilibrium. Plotted is the logarithmic modulus $\ln |\widehat{Q}_k(\omega)|^2$ with its magnitude color coded. The parameters are $\alpha' = 1$, $\beta = 4$ and $H/N = 0.98$. (b) Peak locations of $C_p(n, t)$ versus time t. (c) Decay of the amplitude of correlation functions in time. (d) Scaling of the spatial profile of $C_p(n, t)$. The fitting parameter α is 1.6 and D is 0.33.

scaled $C_p(n, t)$ is also predicted to possess a Gaussian profile from our theory[5]. Therefore, the turbulence of the $\alpha\beta$-FPU chain can also be well characterized by an embedded effective linear stochastic structure.

From above results we can see that there is rather good agreement between theoretical predictions and numerical simulations, so that the scenario of the linear stochastic dynamic structure is effective in describing the long time dynamics of the wave turbulence in many nonlinear wave systems. In this framework, we can well capture two important features of the dynamics: one is the renormalized dispersion relation, which can deviate substantially from the linear dispersion relation, the other is the spatial profile of the momentum correlation functions $C_p(n, t)$. For β-FPU chains, The Hamiltonian (1) possesses quartic terms of trivial and nontrivial resonances, so that the renormalized dispersion relation is induced by quartic resonant interactions as discussed in our previous work [9]. For the Majda–McLaughlin–Tabak model [32], it is demonstrated that nonlinear wave interactions renormalize the dynamics, leading to a possible destruction of scaling structures in the bare wave systems, and creation of nonlinear resonance quartets in wave systems for which there would be no resonances as predicted by the linear dispersion relation [33]. For the (dispersionless) purely quartic chain, the quartet resonances also play an important role in the renormalization of the dispersion relation. Therefore, the renormalized dispersion relation is closely related to the resonance structures of the system. Moreover, by analyzing the peak locations of the integral (7), we have demonstrated that the traveling velocity of $C_p(n, t)$ is exactly the same as the renormalization factor η_L.

After applying the Markovian approximation and thermodynamical limit, the momentum correlation function $C_p(n, t)$ (equation (7)) can be naturally derived. For FPU chains and coupled rotator models, the integral (7) is asymptotically dominated by the small wavenumber k, so that the long time spatiotemporal dynamics is dominated by long-wavelength renormalized waves. This can be seen from the excellent agreement between $|C_p|$ and $|C_p^l|$ as shown in figures 3(b), 5(c), 6(b), and 7(c). In addition, we can obtain the Gaussian profile of $C_p(n, t)$ (equations ((8) and (10)) from the dominance of long-wavelength renormalized waves. This is confirmed in our numerical simulations as shown in figures 3(c), (d), 5(d), 6(c), and 7(d).

[5] Note that from our theory the scaled $C_p(n, t)$ is predicted to possess a Gaussian profile, whereas it is a KPZ function in [18, 19].

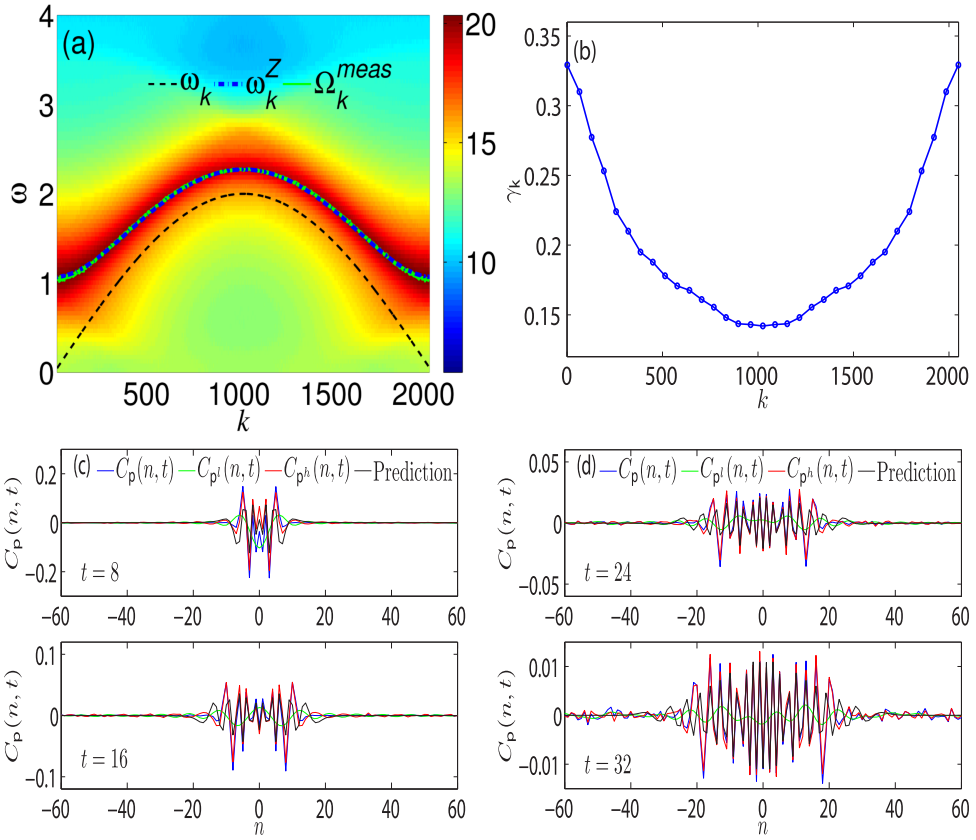

Figure 8. (a) Comparison of dispersion relations ω_k^L (dotted blue line), Ω_k^{meas}(solid green line), and ω_k (dashed black line) for the ϕ^4 model with $N = 2048$ in thermal equilibrium. Plotted is the logarithmic modulus $\ln |\widehat{Q}_k(\omega)|^2$ with its magnitude color coded. The parameters are $\beta = 1$ and $H/N = 1$. (b) The relaxation rate γ_k versus wavenumber k. (c) and (d) comparison of the spatial profile of $C_p(n, t)$ between direct numerical simulations and theoretical prediction (12). The fitting parameter $\omega_{k_0}^Z = 2.27$, $\omega_{k_0}^{Z''} = -4 \times 10^{-6}$, $\gamma_{k_0} = 0.14$, and $\gamma''_{k_0} = 4.9 \times 10^{-7}$.

To go beyond momentum-conserving nonlinear lattices as discussed above, we now turn to the discrete ϕ^4 model with a non-vanishing external on-site potential, which belongs to the class of momentum-nonconserving lattices. The Hamiltonian is $H = \sum_{n=-N/2+1}^{N/2} \frac{1}{2}p_n^2 + \frac{1}{2}(q_{n+1} - q_n)^2 + \frac{\beta}{4}q_n^4$, which possesses a normal heat conduction [14]. Since its total momentum is no longer a constant, the dispersion relation does not vanish, i.e., $\omega_k \neq 0$ at $k = 0$. In our framework of the effective linear stochastic structure, the theoretical prediction of the dispersion relation ω_k^Z (equation (3)) can still well capture the measured dispersion relation in numerical simulations as shown in figure 8(a). The momentum correlation function can be derived as

$$C_p(n, t) = \frac{1}{N} \sum_{k=-N/2+1}^{N/2} e^{-\frac{\gamma_k}{2}t} \left[\cos \widetilde{\omega}_k^Z t - \frac{\gamma_k}{2\widetilde{\omega}_k^Z} \sin \widetilde{\omega}_k^Z t \right] \cos kn, \tag{12}$$

where $\widetilde{\omega}_k^Z = \sqrt{(\omega_k^Z)^2 - \gamma_k^2/4}$. We can see from figure 8(b) that the relaxation rate γ_k has a global minimum at $k = N/2$. Therefore, the long time dynamics of the correlation function $C_p(n, t)$ is dominated by short-wavelength renormalized waves (figures 8(c) and (d)). To evaluate $C_p(n, t)$ of equation (12), we use the quadratic approximation, $\omega_k^Z \approx \omega_{k_0}^Z + \omega_{k_0}^{Z''}(k - k_0)^2/2$ and $\gamma_k \approx \gamma_{k_0} + \gamma''_{k_0}(k - k_0)^2/2$ at $k_0 = N/2$. The parameter values of $\omega_{k_0}^Z$, $\omega_{k_0}^{Z''}$, γ_{k_0}, and γ''_{k_0} can be extracted from the profile of ω_k^Z and γ_k. The above evaluated correlation (black curve) is shown in figures 8(c) and (d) in comparison with direct numerical simulations of $C_p(n, t)$, $C_{p^l}(n, t)$, and $C_{p^h}(n, t)$. It can be seen that the theoretical prediction can approximately capture $C_p(n, t)$ particularly well at the center region around $n = 0$. Because the evaluated correlation (equation (12)) depends only on the local information of ω_k^Z and γ_k at $k = N/2$, this further confirms that short-wavelength renormalized waves are responsible for the long time dynamics of the ϕ^4 model. From above discussions, we can see that for momentum-conserving lattices, the long time dynamics are dominated by long-wavelength renormalized waves whereas for momentum-nonconserving ϕ^4 lattice, the long time dynamics is dominated by short-wavelength renormalized waves.

Finally, we provide an example to show that the scenario of such effective linear stochastic dynamics can be extended to turbulent states in 2D wave systems. We consider a planar square lattice of the β-FPU type with the

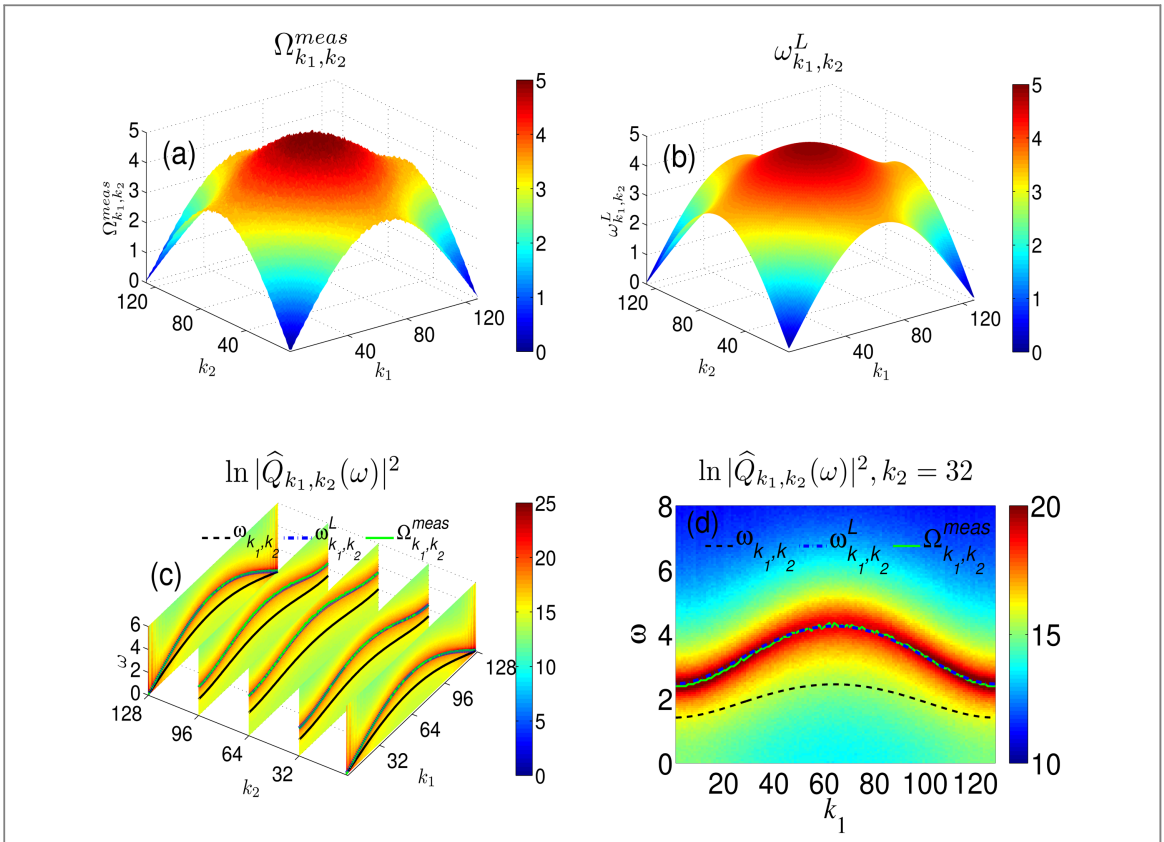

Figure 9. Comparison of (a) measured dispersion relation $\Omega^{\rm meas}_{k_1,k_2}$ and (b) theoretical prediction of renormalized dispersion relation $\omega^{L}_{k_1,k_2}$ for the 2D β-FPU lattice in thermal equilibrium. The logarithmic modulus $\ln|\widehat{Q}_{k_1,k_2}(\omega)|^2$ with its magnitude color coded (c) at $k_2 = 2,\ 32,\ 64,\ 96,\ 128$ and (d) at $k_2 = 32$. In panels (c) and (d), also plotted are ω_{k_1,k_2} (dashed black line), $\omega^{L}_{k_1,k_2}$ (dashed–dotted blue line), $\Omega^{\rm meas}_{k_1,k_2}$ (solid green line) for comparison. The parameters are $N = 128$, $\beta = 1$, and $H/N^2 = 4$. It can be seen that there is a good agreement between the measured $\Omega^{\rm meas}_{k_1,k_2}$ and the theoretical prediction $\omega^{L}_{k_1,k_2}$.

Hamiltonian $H = \sum_{n_1,n_2=-N/2+1}^{N/2} \frac{1}{2}p^2_{n_1,n_2} + \frac{1}{2}(q_{n_1+1,n_2} - q_{n_1,n_2})^2 + \frac{1}{2}(q_{n_1,n_2+1} - q_{n_1,n_2})^2 + \frac{\beta}{4}(q_{n_1+1,n_2} - q_{n_1,n_2})^4 + \frac{\beta}{4}(q_{n_1,n_2+1} - q_{n_1,n_2})^4$. Here, p_{n_1,n_2} and q_{n_1,n_2} are the momentum and displacement of the particle at $(n_1,\ n_2)$, respectively, and β again parameterizes the strength of quartic nonlinearity. The bare linear dispersion relation is $\omega_{k_1,k_2} = [4\sin^2(k_1\pi/N) + 4\sin^2(k_2\pi/N)]^{1/2}$. By invoking the energy equipartition theorem, the renormalized dispersion relation $\omega^{L}_{k_1,k_2}$ can be written as $\omega^{L}_{k_1,k_2} = \sqrt{\langle K\rangle/\langle U\rangle}\,\omega_{k_1,k_2}$, where $K = \sum_{n_1,n_2=-N/2+1}^{N/2} p^2_{n_1,n_2}/2$ and $U = \sum_{n_1,n_2=-N/2+1}^{N/2}(q_{n_1+1,n_2} - q_{n_1,n_2})^2/2 + (q_{n_1,n_2+1} - q_{n_1,n_2})^2/2$ are the kinetic and quadratic potential energy, respectively. For fixed k_1 and k_2, the measured dispersion relation $\Omega^{\rm meas}_{k_1,k_2}$ corresponds to the value of ω on the $\omega - k$ plane where the spatiotemporal spectrum $|\widehat{Q}_{k_1,k_2}(\omega)|^2$ reaches its maximum value (figure 9(a)). Here, $\widehat{Q}_{k_1,k_2}(\omega)$ is the spatiotemporal Fourier transform of $q_{n_1,n_2}(t)$. It can be seen from figure 9 that the theoretical prediction $\omega^{L}_{k_1,k_2}$ agrees well with the measured $\Omega^{\rm meas}_{k_1,k_2}$. Therefore, it can be expected that the turbulence of the 2D β-FPU lattice can also be well captured by the effective linear stochastic dynamics controlled by the renormalized dispersion relation $\omega^{L}_{k_1,k_2}$.

Acknowledgments

This work is supported by Shanghai 14JC1403800, 15JC1400104 and SJTU-UM Collaborative Research Program (DC, DZ), Shanghai Rising Star Program-15QA1402600 and NSFC 91230202 (DZ), 31571071 (DC) and the NYU Abu Dhabi Research Institute G1301.

References

[1] Zakharov V E, L'vov V S and Falkovich G 1992 *Kolmogorov Spectra of Turbulence* (Berlin: Springer)
[2] Gershgorin B, Lvov Y V and Cai D 2005 *Phys. Rev. Lett.* **95** 264302
[3] Gershgorin B, Lvov Y V and Cai D 2007 *Phys. Rev.* E **75** 046603
[4] Li N, Tong P and Li B 2006 *Europhys. Lett.* **75** 49
[5] Li N and Li B 2007 *Europhys. Lett.* **78** 34001

[6] Lee W, Kovačič G and Cai D 2013 *Proc. Natl Acad. Sci.* **110** 3237–41
[7] Alabiso C, Casartelli M and Marenzoni P 1995 *J. Stat. Phys.* **79** 451–71
[8] Alabiso C and Casartelli M 2001 *J. Phys. A: Math. Gen.* **34** 1223
[9] Jiang S X W, Lu H H, Zhou D and Cai D 2014 *Phys. Rev.* E **90** 032925
[10] Fermi E, Pasta J and Ulam S 1955 Studies of nonlinear problems *Los Alamos Scientific Lab., N. Mex.* LA-1940
[11] Ford J 1992 *Phys. Rep.* **213** 271–310
[12] Bonetto F, Lebowitz J L and Rey-Bellet L 2000 *Mathematical Physics 2000* ed A Fokas *et al* (London: Imperial College Press) pp 128–50
[13] Lepri S 1998 *Phys. Rev.* E **58** 7165
[14] Lepri S, Livi R and Politi A 2003 *Phys. Rep.* **377** 1–80
[15] Dhar A 2008 *Adv. Phys.* **57** 457–537
[16] Li N, Li B and Flach S 2010 *Phys. Rev. Lett.* **105** 054102
[17] Zhao H 2006 *Phys. Rev. Lett.* **96** 140602
[18] Mendl C B and Spohn H 2013 *Phys. Rev. Lett.* **111** 230601
[19] Spohn H 2014 *J. Stat. Phys.* **154** 1191–227
[20] Das S G, Dhar A, Saito K, Mendl C B and Spohn H 2014 *Phys. Rev.* E **90** 012124
[21] Mori H 1965 *Progr. Theoret. Phys.* **33** 423–55
[22] Zwanzig R 2001 *Nonequilibrium Statistical Mechanics* (Oxford: Oxford University Press)
[23] Giacomelli G, Hegger R, Politi A and Vassalli M 2000 *Phys. Rev. Lett.* **85** 3616
[24] Narayan O and Ramaswamy S 2002 *Phys. Rev. Lett.* **89** 200601
[25] Pereverzev A 2003 *Phys. Rev.* E **68** 056124
[26] van Beijeren H 2012 *Phys. Rev. Lett.* **108** 180601
[27] Delfini L, Lepri S, Livi R and Politi A 2006 *Phys. Rev.* E **73** 060201
[28] Delfini L, Lepri S, Livi R and Politi A 2007 *J. Stat. Mech.* P02007
[29] Frizzera W, Monteil A and Capobianco J 1998 *Il Nuovo Cimento* D **20** 1715–34
[30] Gendelman O and Savin A 2000 *Phys. Rev. Lett.* **84** 2381
[31] Giardinà C Livi R, Politi A and Vassalli M 2000 *Phys. Rev. Lett.* **84** 2144
[32] Majda A J, McLaughlin D W and Tabak E G 1997 *J. Nonlinear Sci.* **7** 9–44
[33] Lee W, Kovačič G and Cai D 2009 *Phys. Rev. Lett.* **103** 024502